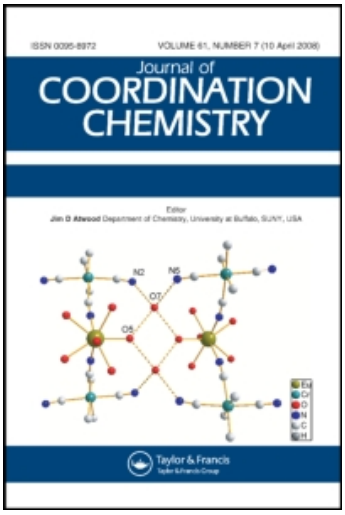

Journal of Coordination Chemistry
Publication details, including instructions for authors and subscription information:
http://www.informaworld.com/smpp/title~content=t713455674

Synthesis, structures and magnetic properties of nickel bis(dithiolene) complexes with $[Fe(qsal)_2]^+$

Xiao-Ming Li[a]; Yong Ji[a]; Cai-Feng Wang[a]; Jing-Lin Zuo[a]; Xiao-Zeng You[a]
[a] State Key Laboratory of Coordination Chemistry, School of Chemistry and Chemical Engineering, Nanjing National Laboratory of Microstructures, Nanjing University, Nanjing, China

To cite this Article Li, Xiao-Ming , Ji, Yong , Wang, Cai-Feng , Zuo, Jing-Lin and You, Xiao-Zeng(2009) 'Synthesis, structures and magnetic properties of nickel **bis**(dithiolene) complexes with $[Fe(qsal)_2]^+$', Journal of Coordination Chemistry, 62: 9, 1544 — 1552
To link to this Article: DOI: 10.1080/00958970802669222
URL: http://dx.doi.org/10.1080/00958970802669222

Journal of Coordination Chemistry
Vol. 62, No. 9, 10 May 2009, 1544–1552

Taylor & Francis
Taylor & Francis Group

Synthesis, structures and magnetic properties of nickel *bis*(dithiolene) complexes with $[Fe(qsal)_2]^+$

XIAO-MING LI, YONG JI, CAI-FENG WANG, JING-LIN ZUO* and XIAO-ZENG YOU

State Key Laboratory of Coordination Chemistry, School of Chemistry and Chemical Engineering, Nanjing National Laboratory of Microstructures, Nanjing University, Nanjing, China

(*Received 17 July 2008; in final form 8 August 2008*)

Two new compounds containing the possible Fe(III) spin-crossover cation, $[Fe(qsal)_2]^+$ (qsalH = *N*-(8-quinolyl)salicylaldimine), and nickel *bis*(dithiolene) anions have been synthesized. Both are 1 : 1 salts $[Fe(qsal)_2][Ni(dddt)_2] \cdot CH_3CN \cdot CH_3OH$ (**1**) and $[Fe(qsal)_2][Ni(pddt)_2]$ (**2**) (dddt = 5,6-dihydro-1,4-dithiin-2,3-dithiolate; pddt = 6,7-dihydro-5H-1,4-dithiepin-2,3-dithiolate). They have been characterized by X-ray crystal structure determination, elemental analysis, UV-Vis spectra and magnetic susceptibility measurements. The UV–Vis spectra are dominated by $[Ni(L)_2]^-$ (**1**, L = dddt; **2**, L = pddt). Magnetic studies show antiferromagnetic interaction in **1** from intermolecular S···S contacts and π–π stacking interactions, while the antiferromagnetic interaction in **2** is very weak.

Keywords: Nickel *bis*(dithiolene) complexes; Iron complexes; Crystal structures; Magnetic properties

1. Introduction

Attention has focused on multi-functional molecular materials combining components with different properties, especially for conductive and magnetic materials [1–4]. Nickel complexes of 1,2-dithiolene, for example $[Ni(L)_2]^-$ (**1**, L = 5,6-dihydro-1,4-dithiin-2,3-dithiolate (dddt); **2**, L = 6,7-dihydro-5H-1,4-dithiepin-2,3-dithiolate (pddt)), possess an extended electronically delocalized structure required for electron conduction. They are also used in hybrid materials because of the unusual NIR properties, the unique redox activity, electrical, and magnetic behavior [5–11]. Spin-crossover (SCO) transition metal complexes [12–19], such as $[Fe(qsal)_2]^+$ (qsalH = *N*-(8-quinolyl)salicylaldimine), have been well studied [13, 15]; the counteranions affect their magnetic properties. To search for new multi-functional molecular materials with conducting metal *bis*(dithiolene) and SCO Fe(III) complexes, we synthesized two new cation/anion compounds, $[Fe(qsal)_2][Ni(dddt)_2] \cdot CH_3CN \cdot CH_3OH$ (**1**) and $[Fe(qsal)_2][Ni(pddt)_2]$ (**2**). Their synthesis, crystal structures and magnetic properties are described here.

*Corresponding author. Email: zuojl@nju.edu.cn

Journal of Coordination Chemistry
ISSN 0095-8972 print/ISSN 1029-0389 online © 2009 Taylor & Francis
DOI: 10.1080/00958970802669222

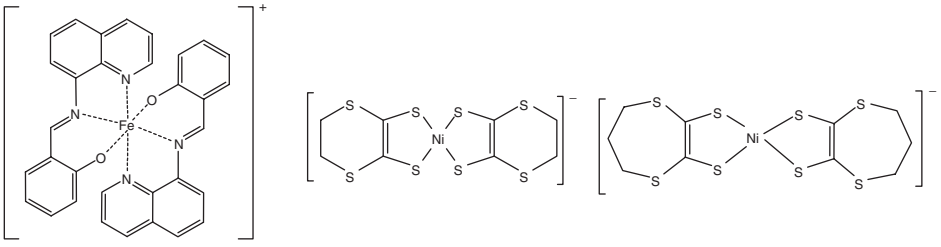

$[Fe(qsal)_2]^+$ $[Ni(dddt)_2]^-$ $[Ni(pddt)_2]^-$

2. Experimental

2.1. *Reagents*

All solvents were of analytical grade and used without purification. $[Fe(qsal)_2]Cl \cdot 1.5H_2O$ was prepared from 8-aminoquinoline and salicylaldehyde according to the previously reported procedures [20, 21]. $[n\text{-}Bu_4N][Ni(dddt)_2]$ and $[n\text{-}Bu_4N][Ni(pddt)_2]$ were synthesized by the methods described in the literature [5, 6, 22, 23].

2.2. *Synthesis*

2.2.1. Synthesis of $[Fe(qsal)_2][Ni(dddt)_2] \cdot CH_3CN \cdot CH_3OH$ (1). A solution of $[Fe(qsal)_2]Cl \cdot 1.5H_2O$ (11.7 mg, 0.02 mmol) in 5 mL of acetonitrile was mixed with a solution of $[n\text{-}Bu_4N][Ni(dddt)_2]$ (13.2 mg, 0.02 mmol) in 3 mL of acetonitrile, and immediately a dark-brown solution was obtained. Black crystals formed by diffusion of ether vapor into this solution over a few days. Anal. Calcd for $C_{40}H_{30}O_2N_4S_8NiFe$ (%): C, 49.54; H, 3.12; N, 5.78; S, 26.45. Found (%): C, 49.59; H, 3.23; N, 5.67; S, 26.34. Selected IR (cm^{-1}): 1360, 1430, 1601, 826.

2.2.2. Synthesis of $[Fe(qsal)_2][Ni(pddt)_2]$ (2). The method for preparing **2** was similar to that for **1**. Anal. Calcd for $C_{42}H_{34}O_2N_4S_8NiFe$ (%): C, 50.56; H, 3.43; N, 5.61; S, 25.71. Found (%): C, 50.49; H, 3.41; N, 5.68; S, 25.71. Selected IR (cm^{-1}): 1380, 1429, 1601, 830.

2.3. *General procedures*

Elemental analyses for C, H, N, and S were performed on a Perkin-Elmer 240C analyzer. IR spectra were taken on a Vector22 Bruker spectrophotometer (400–4000 cm^{-1}) with KBr pellets. UV–Vis absorption spectra were recorded on a Shimadzu UV-3100 spectrometer. The magnetic susceptibilities were measured using a Quantum Design MPMS-XL7 SQUID magnetometer from 1.8 to 300 K.

2.4. *X-ray crystallography*

The crystal structures of **1** and **2** were determined on a Siemens (Bruker) SMART CCD diffractometer using monochromated Mo-Kα radiation ($\lambda = 0.71073$ Å) at

Table 1. Crystallographic data for **1** and **2**.

	1	**2**
Empirical formula	$C_{43}H_{39}FeN_5NiO_4S_8$	$C_{42}H_{34}FeN_4NiO_2S_8$
Formula weight	1060.83	997.77
Temperature (K)	298(2)	298(2)
Wavelength (Å)	0.71073	0.71073
Crystal system	Monoclinic	Monoclinic
Space group	$P2_1/c$	$P2_1/n$
Unit cell dimensions (Å, °)		
a	14.004(5)	10.384(3)
b	16.053(5)	33.807(8)
c	21.356(7)	11.747(3)
α	90.00	90.00
β	99.691(8)	90.856(5)
γ	90.00	90.00
V (Å^3)	4733(3)	4123.4(19)
Z	4	4
D_{Calcd} (Mg m^{-3})	1.489	1.607
Absorption coefficient (mm^{-1})	1.104	1.258
$F(000)$	2184	2048
Crystal size (mm^3)	$0.23 \times 0.16 \times 0.13$	$0.24 \times 0.23 \times 0.21$
θ range (°)	1.60–26.00	1.84–26.00
Index range (h, k, l)	$-11 \le h \le 17$, $-19 \le k \le 19$, $-23 \le l \le 26$	$-12 \le h \le 12$, $-32 \le k \le 41$, $-14 \le l \le 14$
Reflections collected	24988	22117
Independent reflections	9289 [$R_{(int)} = 0.1073$]	8098 [$R_{(int)} = 0.0483$]
Refinement method	Full-matrix least-squares on F^2	Full-matrix least-squares on F^2
Data/restraints/parameters	9289/339/559	8098/4/533
Goodness-of-fit on F^2	1.017	1.002
Final R indices [$I > 2\sigma(I)$]	$R_1 = 0.1111$, $wR_2 = 0.1997$	$R_1 = 0.0393$, $wR_2 = 0.0638$
R indices (all data)	$R_1 = 0.2185$, $wR_2 = 0.2447$	$R_1 = 0.0666$, $wR_2 = 0.0659$
Largest difference peak and hole (e Å^{-3})	0.697 and −0.532	0.605 and −0.463

room temperature. Cell parameters were retrieved using SMART software and refined using SAINT [24] on all observed reflections. Data were collected using a narrow-frame method with scan widths of 0.30° in ω and an exposure time of 10 s per frame. The highly redundant data sets were reduced using SAINT and corrected for Lorentz and polarization effects. Absorption corrections were applied using SADABS [25] supplied by Bruker. Structures were solved by direct methods using SHELXL-97 [26]. The positions of the metals were located from direct-method E maps; other nonhydrogen atoms were found using alternating difference Fourier syntheses and least-square refinement cycles and, during the final cycles, were refined anisotropically. Hydrogen atoms were placed in calculated positions and refined as riding atoms with a uniform value of U_{iso}. Information concerning crystallographic data collection and structure refinement is summarized in table 1. CCDC-694848 (**1**) and CCDC-694849 (**2**) contain the supplementary crystallographic data for this article.

3. Results and discussion

3.1. *Crystal structures*

The molecular structures of **1** and **2** with atom numbering scheme are shown in figures 1 and 2, respectively. Selected bond lengths and angles of the complexes are listed

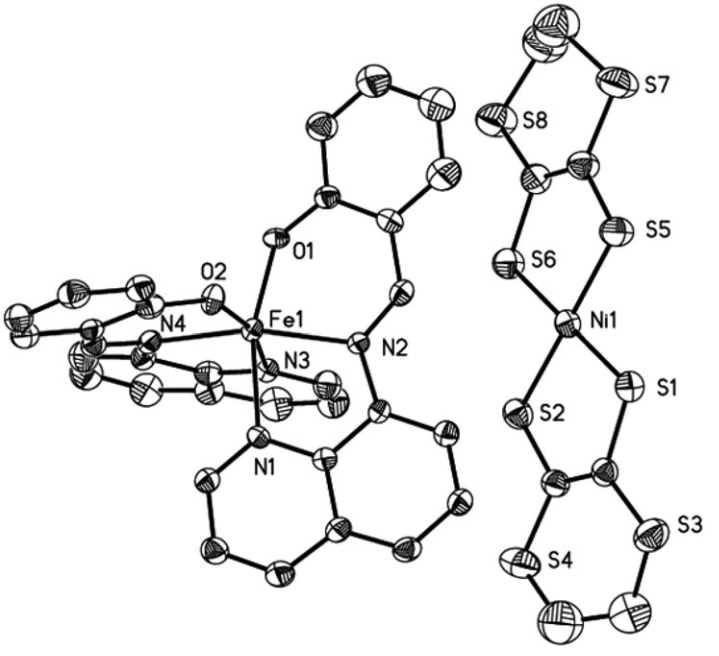

Figure 1. ORTEP of **1** with atom numbering scheme; hydrogen atoms and solvated molecules are omitted for clarity. Ellipsoids are drawn at 30% probability.

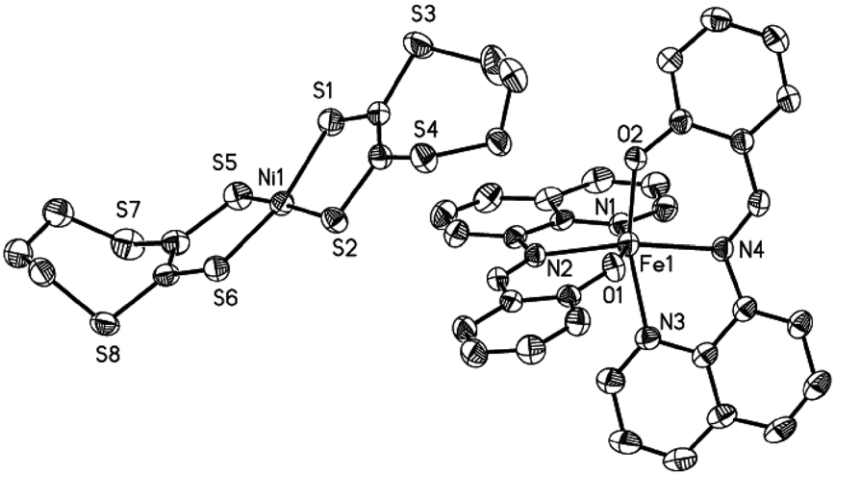

Figure 2. ORTEP of **2** with atom numbering scheme; hydrogen atoms and solvated molecules are omitted for clarity. Ellipsoids are drawn at 30% probability.

in table 2. The asymmetric unit of **1** consists of a $[Fe(qsal)_2]^+$ and $[Ni(dddt)_2]^-$, while the counteranion in **2** is $[Ni(pddt)_2]^-$. In both **1** and **2**, the Fe(III) is a distorted octahedral geometry, with four nitrogens and two oxygens from two $qsal^-$ ligands. As listed in table 2, the average bond distances of Fe–O [1.901(1) Å for **1** and 1.894(3) Å for **2**] and Fe–N [2.135(0) Å for **1** and 2.130(7) Å for **2**] are longer than those observed in low-spin Fe(III) cases, and close to those reported for the high-spin Fe(III) compounds [14, 17].

Table 2. Selected bond distances (Å) and angles (°) for **1** and **2**.

		1	
Fe(1)–O(1)	1.897(6)	Fe(1)–O(2)	1.904(6)
Fe(1)–N(2)	2.100(7)	Fe(1)–N(4)	2.105(8)
Fe(1)–N(3)	2.161(7)	Fe(1)–N(1)	2.171(7)
Ni(1)–S(2)	2.129(3)	Ni(1)–S(5)	2.135(4)
Ni(1)–S(6)	2.140(3)	Ni(1)–S(1)	2.148(3)
O(1)–Fe(1)–O(2)	94.5(3)	O(2)–Fe(1)–N(3)	164.0(3)
N(3)–Fe(1)–N(1)	86.9(3)	O(1)–Fe(1)–N(2)	87.5(3)
N(2)–Fe(1)–N(3)	93.1(3)	S(2)–Ni(1)–S(5)	178.82(15)
O(2)–Fe(1)–N(2)	102.1(3)	N(4)–Fe(1)–N(3)	76.5(3)
S(2)–Ni(1)–S(6)	87.30(13)	O(1)–Fe(1)–N(4)	102.9(3)
O(1)–Fe(1)–N(1)	163.1(3)	S(5)–Ni(1)–S(6)	91.52(13)
O(2)–Fe(1)–N(4)	87.7(3)	O(2)–Fe(1)–N(1)	91.9(3)
S(2)–Ni(1)–S(1)	91.34(13)	N(2)–Fe(1)–N(4)	165.2(3)
N(2)–Fe(1)–N(1)	75.9(3)	S(5)–Ni(1)–S(1)	89.83(13)
O(1)–Fe(1)–N(3)	91.1(3)	N(4)–Fe(1)–N(1)	93.0(3)
S(6)–Ni(1)–S(1)	177.02(14)		
		2	
Fe(1)–O(1)	1.8909(19)	Fe(1)–O(2)	1.8978(19)
Fe(1)–N(4)	2.088(2)	Fe(1)–N(2)	2.105(2)
Fe(1)–N(1)	2.154(2)	Fe(1)–N(3)	2.175(2)
Ni(1)–S(6)	2.1328(9)	Ni(1)–S(1)	2.1340(10)
Ni(1)–S(2)	2.1391(9)	Ni(1)–S(5)	2.1417(9)
O(1)–Fe(1)–O(2)	99.54(9)	O(2)–Fe(1)–N(1)	86.13(9)
N(1)–Fe(1)–N(3)	89.48(8)	O(1)–Fe(1)–N(4)	94.22(8)
N(4)–Fe(1)–N(1)	100.03(9)	S(6)–Ni(1)–S(1)	164.10(4)
O(2)–Fe(1)–N(4)	87.68(9)	N(2)–Fe(1)–N(1)	76.90(9)
S(6)–Ni(1)–S(2)	89.85(3)	O(1)–Fe(1)–N(2)	88.15(8)
O(1)–Fe(1)–N(3)	88.96(8)	S(1)–Ni(1)–S(2)	90.93(4)
O(2)–Fe(1)–N(2)	102.85(8)	O(2)–Fe(1)–N(3)	162.62(9)
S(6)–Ni(1)–S(5)	91.30(4)	N(4)–Fe(1)–N(2)	168.69(9)
N(4)–Fe(1)–N(3)	76.53(10)	S(1)–Ni(1)–S(5)	90.15(4)
O(1)–Fe(1)–N(1)	164.89(9)	N(2)–Fe(1)–N(3)	92.49(9)
S(2)–Ni(1)–S(5)	171.92(4)		

The Ni atom is coordinated by four sulfurs from two 1,2-dithiolene ligands (dddt for **1** and pddt for **2**) with the average Ni–S bond length of 2.138(3) Å for **1** and 2.137(1) Å for **2**. The Ni(II) is almost coplanar with the four coordinated sulfurs in **1**, but in **2**, the dihedral angle between planes of Ni1, S1, S2 and Ni1, S5, S6 is 17.7°.

In **1**, as shown in figure 3, a short intermolecular S···S contact (S4···S4 (#1), the symmetry operation #1: $1-x$, $1-y$, $1-z$) with distance of 3.643 Å is found in $[Ni(dddt)_2]^-$, which is less than the sum of the van der Waal's radii of sulfur (3.70 Å) [7]. Moreover, there are π–π stacking interactions between two aromatic rings (N1 and C1−C5 *vs*. N3 and C17−C21, 3.705 Å), which lead to the formation of a one-dimensional chain along *b*. However, no appreciable intermolecular interactions are observed in **2** (figure 4).

3.2. *UV–Vis absorption spectra*

The UV–Vis absorption spectra of **1** and **2**, along with precursors $[n\text{-}Bu_4N][Ni(dddt)_2]$ and $[n\text{-}Bu_4N][Ni(pddt)_2]$ in acetonitrile, are shown in figure 5. Complex **1** exhibits three characteristic absorption peaks at 317, 406, and 1175 nm. Similar to **1**, bands of **2** are 327, 398, and 927 nm, respectively. Peaks at high energy ($\lambda = 317$ and 406 nm for **1** and

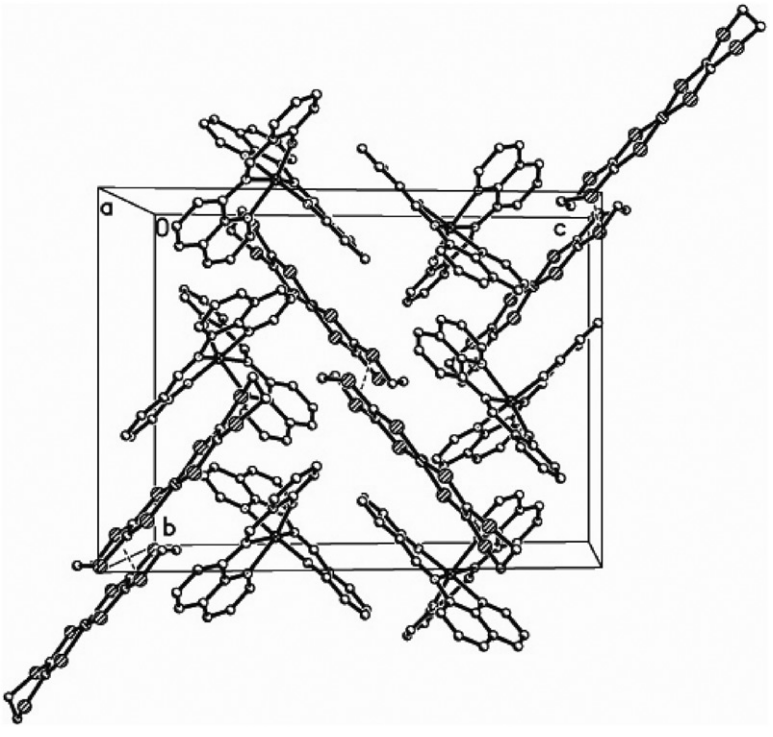

Figure 3. Cell packing diagram of **1** along the *a*-axis (dotted line represents S···S non bonded contacts <3.7 Å).

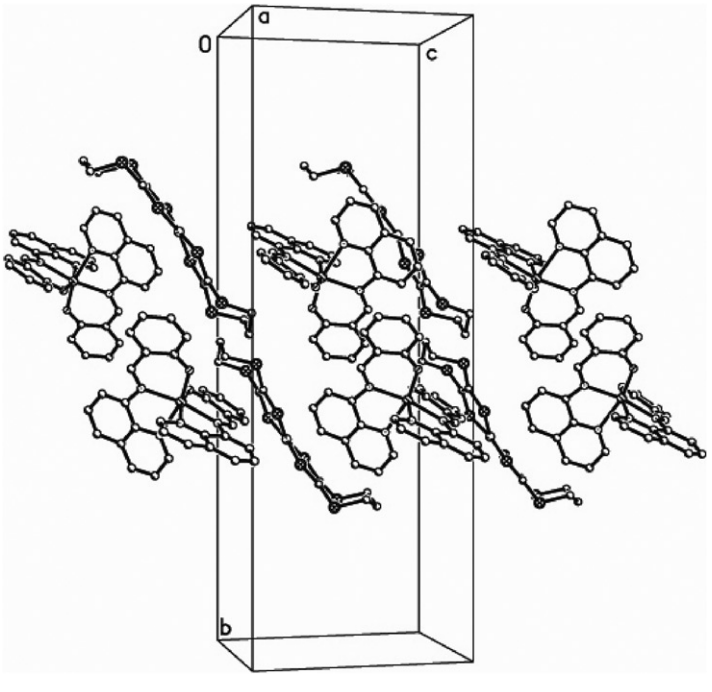

Figure 4. Cell packing diagram of **2** along *a*.

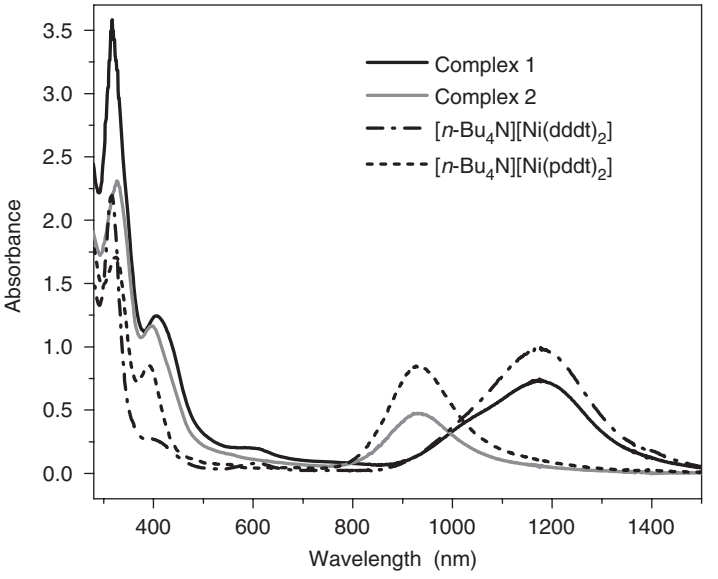

Figure 5. UV–Vis absorption of $[Fe(qsal)_2][Ni(dddt)_2]\cdot CH_3CN\cdot CH_3OH$ (**1**) and $[Fe(qsal)_2][Ni(pddt)_2]$ (**2**) in acetonitrile ($5\times10^{-5}\,mol\cdot L^{-1}$), as well as $[n\text{-}Bu_4N][Ni(dddt)_2]$ and $[n\text{-}Bu_4N][Ni(pddt)_2]$.

$\lambda = 327$ and 398 nm for **2**) are assigned to the $L(\pi)\rightarrow L(\pi^*)$ transitions of the anion, and the peaks at 1175 nm for **1** and 927 nm for **2** are due to $\pi\rightarrow\pi^*$ of the anions [6–11]. The absorption peaks in **1** and **2** have no significant shift in comparison with those in the relevant precursors, suggesting the $[Fe(qsal)_2]^+$ cation has negligible effects on the electronic structure of $[Ni(dddt)_2]^-$ and $[Ni(pddt)_2]^-$.

3.3. *Magnetic properties of the complexes*

Variable temperature magnetic susceptibilities for **1** and **2** were measured on a Quantum Design MPMS-XL7 SQUID magnetometer from 1.8 to 300 K. For **1**, as shown in figure 6, the value of $\chi_M T$ at room temperature is 4.25 emu K mol^{-1}, slightly lower than the expected spin-only value of 4.75 emu K mol^{-1} for a high-spin Fe(III) and low-spin Ni(III) ($g_{Fe}=g_{Ni}=2$, $S_{Fe}=5/2$ and $S_{Ni}=1/2$). The $\chi_M T$ value decreases significantly as the temperature lowers and reaches a value of 1.72 emu K mol^{-1} at 1.8 K, implying the existence of antiferromagnetic coupling in **1**. A fit of the data to the Curie–Weiss law in the temperature range 22–300 K gives a Curie constant $C = 3.39$ emu K mol^{-1} and Weiss constant $\theta = -27.07$ K. The antiferromagnetic interaction in **1** can be ascribed to intermolecular interactions since the shorter intermolecular S···S contact between anions and π–π stacking interaction between cations exist. However, the value of $\chi_M T$ for **2** remains almost constant at ~3.911 emu K mol^{-1} in the temperature range 40–300 K (figure 7). When the temperature is below 40 K, the $\chi_M T$ value decreases slowly as the temperature decreases and reaches 1.97 emu K mol^{-1} at 1.8 K, which can be attributed to very weak intermolecular antiferromagnetic interactions. The $1/\chi_M$ *versus* T data for **2** are nearly linear in the whole temperature range and the fit to Curie-Weiss law yields $C = 3.93$ emu K mol^{-1} and $\theta = -2.28$ K. A structurally similar complex reported

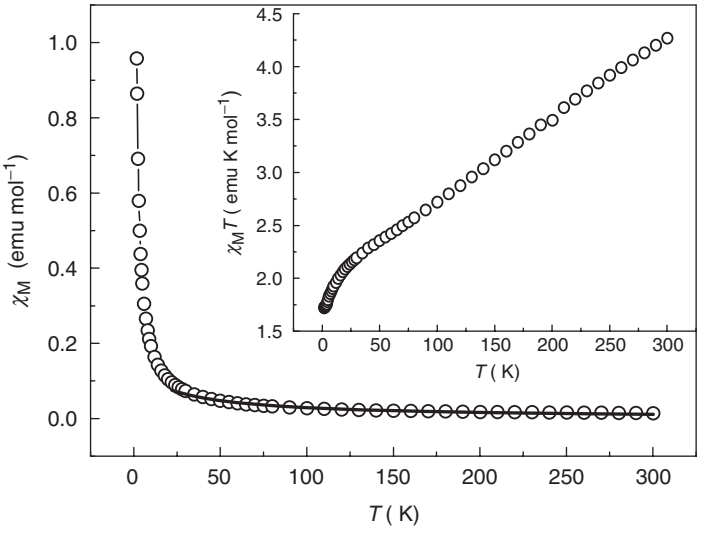

Figure 6. Temperature dependence of χ_M and $\chi_M T$ for **1**. Solid lines represent fits to the data.

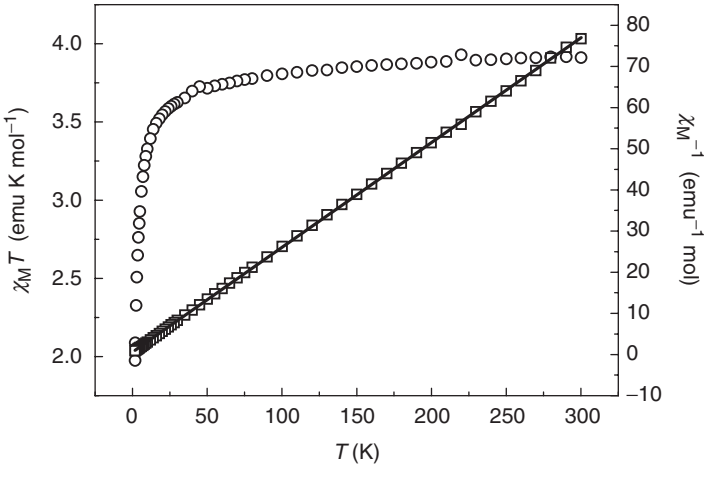

Figure 7. Temperature dependence of χ_M and $\chi_M T$ for **2**. Solid lines represent fits to the data.

previously ($[Fe(qsal)_2][Ni(dmit)_2] \cdot 2CH_3CN$) exhibits SCO phenomenon [14], but no SCO behavior was detected in **1** and **2**, which is reasonable because SCO is very sensitive to small changes of structure and components.

Acknowledgments

This work was supported by the Major State Basic Research Development Program (2006CB806104) and the National Science Foundation of China (Grant 20725104).

References

[1] E. Coronado, J.R. Galán-Mascarós, C.J. Gómez-García, V. Laukhin. *Nature*, **408**, 447 (2000).
[2] S. Dorbes, L. Valade, J.A. Real, C. Faulmann. *Chem. Commun*., 69 (2005).
[3] K. Takahashi, H.B. Cui, Y. Okano, H. Kobayashi, Y. Einaga, O. Sato. *Inorg. Chem*., **45**, 5739 (2006).
[4] C. Faulmann, K. Jacob, S. Dorbes, S. Lampert, I. Malfant, M.L. Doublet, L. Valade, J.A. Real. *Inorg. Chem*., **46**, 8548 (2007).
[5] A.J. Schultz, H.H. Wang, L.C. Soderholm, T.L. Sifter, J.M. Williams, K. Bechgaard, M.H. Whangbo. *Inorg. Chem*., **26**, 3757 (1987).
[6] J.F. Bai, J.L. Zuo, W.L. Tan, W. Ji, Z. Shen, H.K. Fun, K. Chinnakali, I.A. Razak, X.Z. You, C.M. Che. *J. Mater. Chem*., **9**, 2419 (1999).
[7] Y. Ji, M. Xu, W. Liu, H.K. Fun, J.L. Zuo, X.Z. You. *J. Coord. Chem*., **58**, 1573 (2005).
[8] T.M. Yao, J.L. Zuo, X.Z. You, X.Y. Huang. *Polyhedron*, **14**, 1487 (1995).
[9] M. Nomura, T. Cauchy, M. Geoffroy, P. Adkine, M. Fourmigue. *Inorg. Chem*., **45**, 8194 (2006).
[10] H.J. Lee, D.Y. Noh. *Polyhedron*, **19**, 425 (2000).
[11] Y. Ji, J.L. Zuo, L.X. Chen, Y.Q. Tian, Y.L. Song, Y.Z. Li, X.Z. You. *J. Phys. Chem. Solids*, **66**, 207 (2005).
[12] O. Kahn, C. Jay Martinez. *Science*, **279**, 44 (1998).
[13] S. Hayami, Z.Z. Gu, H. Yoshiki, A. Fujishima, O. Sato. *J. Am. Chem. Soc*., **123**, 11644 (2001).
[14] K. Takahashi, H.B. Cui, H. Kobayashi, Y. Einaga, O. Sato. *Chem. Lett*., **34**, 1240 (2005).
[15] S. Hayami, T. Kawahara, G. Juhasz, K. Kawamura, K. Uehashi, O. Sato, Y. Maeda. *J. Radioanal. Nucl. Chem*., **3**, 443 (2003).
[16] C. Faulmann, S. Dorbes, S. Lampert, K. Jacob, B.G. de Bonneval, G. Molnár, A. Bousseksou, J.A. Real, L. Valade. *Inorg. Chim. Acta*, **360**, 3870 (2007).
[17] S. Okamura, Y. Maeda. *J. Radioanal. Nucl. Chem*., **3**, 523 (2003).
[18] L.C.J. Pereira, A.M. Gulamhussen, J.C. Dias, I.C. Santos, M. Almeida. *Inorg. Chim. Acta*, **360**, 3887 (2007).
[19] A.B. Kudryavtsev, G. Frauendienst, W. Linert. *J. Coord. Chem*., **46**, 221 (1998).
[20] H. Oshio, K. Kitazaki, J. Mishiro, N. Kato, Y. Maeda, Y. Takashima. *J. Chem. Soc., Dalton Trans*., 1341 (1987).
[21] R.C. Dickinson, W.A. Baker, R.L. Collons. *J. Inorg. Nucl. Chem*., **39**, 1531 (1977).
[22] X.B. Chi, Y.G. Li, C.S. Jiang. *Chin. J. Synth. Chem*., **10**, 409 (2002).
[23] J.H. Welch, R.D. Bereman, P. Singh. *Inorg. Chim. Acta*, **162**, 89 (1989).
[24] *SAINT-Plus*, version 6.02, Bruker Analytical X-ray System, Madison, WI (1999).
[25] G.M. Sheldrick. *SADABS, An Empirical Absorption Correction Program*, Bruker Analytical X-ray Systems, Madison, WI (1996).
[26] G.M. Sheldrick. *SHELXTL-97*, Universität of Göttingen: Göttingen, Germany (1997).